Proceedings of
ASME Turbo Expo 2012, June 11-15, 2012, Copenhagen, Denmark

GT2012-68148

EFFECTS OF ROTOR TIP CLEARANCE ON TIP CLEARANCE FLOW POTENTIALLY LEADING TO NSV IN AN AXIAL COMPRESSOR

Hong-Sik Im *
Ge-Cheng Zha†
Dept. of Mechanical and Aerospace Engineering
University of Miami
Coral Gables, Florida 33124
E-mail: gzha@miami.edu

ABSTRACT

This paper investigates non-synchronous vibration (NSV) mechanism of a high-speed axial compressor with three different rotor tip clearances. Numerical simulations for $1/7$th annulus periodic sector are performed using an unsteady Reynolds-averaged Navier-Stokes(URANS) solver with a fully conservative sliding boundary condition to capture wake unsteadiness between the rotor and stator blades. The simulated NSV shows that the frequency and amplitude are strongly influenced by the tip clearance size and shape. The predicted NSV frequency is in good agreement with the experiment. The maximum amplitude of the NSV occurs at about 78% span of the rotor suction leading edge regardless of tip clearance due to a strong interaction of incoming flow, tip leakage flow and tip vortex. The instability of tornado like tip vortex oscillating in streamwise direction appears to be the main cause of the NSV observed in this study.

1 Introduction

Turbomachinery aeromechanic problems are very challenging since they involve both aerodynamics and structural vibration. Blade vibration due to forced response and flutter have been studied for decades with the progress of improving turbomachinery efficiency and reliability. Recently, a new turbomachinery aeromechanic problem, namely non-synchronous vibration(NSV), whose blade vibration frequency is away from harmonics of rotor shaft frequency, has attracted a lot of attention [1–8]. The present study shows that NSV has no resonance with the rotor blades, while flutter is a self-excited aeroelastic instability at or close to the rotor blade natural frequency [1, 9].

Rotating instability (RI) is considered as one cause of NSV [1–4]. The experiment for the 10 stage high pressure axial compressor by Baumgartner et al. [1] shows that for a certain operating condition high vibration levels on the first stage blades exist. The frequencies are not in resonance with engine orders. A rotating flow instability revolves relative to the blade row similar to rotating stall cell. The velocity fluctuations measured by the Hot-film probe near the blade trailing edge show the radial dependency of this rotating instability. The frequencies of the rotating instability are visible at 91% blade span with high coherence level, , which is decaying away from the RI center, and eventually at 65% blade span the RI is no more detectable.

Kielb et al. [2] conducted an experimental and numerical investigation for a full size compressor rig where blade-mounted strain gages and case-mounted unsteady pressure transducers are devised to measure the NSV. The experimental strain gage data show step change in frequency as the compressor operating condition varies. This is another feature of the NSV. The stage 1 rotor blades experience a significant NSV response of 2661 Hz at 12700 rpm near first torsional mode (or 2nd mode natural frequency) and exhibit the NSV frequency shift from 2661 to 2600 Hz at 12800 rpm. At the casing, the NSV frequencies of 3516 Hz and 3662 Hz are measured in the non-rotating reference frame. Their numerical results for the 1/7th rotor annulus rotor indicate a suction side vortex shedding and a tip flow instability near 75% span as the excitation source of the NSV.

The work of Marz et al. [3] also shows the rotating instability as a main source for NSV. A low speed single stage

*Ph.D. Student, ASME Member
†Associate Professor, ASME Senior Member

fan with outlet guide vanes is used for their experimental and numerical study on the NSV. The rotor design speed is 3000 rpm and has the blade passing frequency (BPF) of 560Hz. They tested four different tip clearances of 0.7%, 1.4%, 2.8%, and 5.6% tip axial chord at near the maximum fan loading condition. The measured wall pressure spectrum shows a NSV frequency at roughly half of BPF. The time-lapse plots of casing wall pressure indicate that the flow intensity varies from blade to blade with the presence of a high fluctuating flow instability in the rotor entry plane for tip clearances of 2.8% and 5.6%. It turns out that the blade sensor signal near the rotating instability has a strong periodic content. A vortex structure moving from the suction side to the pressure side is observed in the middle of the blade passage by the full annulus simulation for 2.8% tip clearance, which is the main causes of unsteadiness when the rotating instability develops. The numerical study shows no tip spillage flow even with the rotating instability.

Mailach et al. [4] carried out an experimental study of a low speed research compressor to investigate influence of tip clearance and operating point on rotating instability. Rotating instability have been found at a tip clearance of 3% tip axial chord. At a larger tip clearance of 4.3%, the rotating instability is fully developed for all the rotor speeds including 50%, 80%, and 100% design speed. The formation of rotating instability is limited to a narrow operating range near the stall boundary. The measurement at the casing wall shows a narrow band increase of the amplitudes in the frequency spectrum at about 30% of BPF. When the compressor approaches the stall boundary, the rotating instability shifts to slightly lower frequencies while amplitude of the perturbation grows. Measurements on the rotor blades show that the rotating instability is limited to the blade tip region. Maximum amplitudes appear at 92% of the blade height and 20% to 30% of chord length. For a large tip clearance a strong blade tip vortex is observed in the rotor tip region. The fluctuating blade tip vortices propagate in rotor circumferential direction. Tip clearance size is shown as the main influence parameter on the rotating instability.

Thomassin, et al. [5,6] suggested a theory different from the rotating instability to explain the NSV based on the resonance of a impinging jet vortex structure and the acoustic feedback of a vibrating plate. The jet core feedback theory has been proved by an experiment conducted in [5, 6]. It shows that when the acoustic reflection wave length equals to the jet-to-plate distance, the jet vortical structures lock-on to the acoustic wave frequency and significant amplification of the pressure fluctuation and vibration of the flexible plate are observed. They suggest a simple model to predict the critical tip velocity based on their impinging jet experiment. Vo [8]'s simulation shows a tip clearance flow instability for an isolated subsonic axial compressor rotor. In the blade tip region the trailing edge backflow causes flow impingement on the pressure side that leads to the flow unsteadiness associated with the NSV.

Note that the effect of blade motion of NSV is not taken into account in this study. The numerical studies [2, 3, 5, 6] show that the flow instabilities such as rotating instability (RI) and tip leakage acoustic resonance captured without considering fluid-structure interaction are sufficient to predict the measured NSV frequencies.

It is clear that NSV occurs mostly in the tip region due to the instability associated with tip clearance flows. The purpose of this paper is to study the effect of tip clearance on non-synchronous blade vibration. Three different tip clearances are used in this tip sensitivity study as shown in Fig. 1. Tip clearance 1 is designed with a plain rotor tip of 2.4% C_t(tip chord), tip clearance 2 with a plain tip of 1.1% C_t, and tip clearance 3 with a convex type pinched tip of 1.1% C_t around tip center and 2.4%C_t near the rotor tip LE/TE. These three tip clearance shapes correspond to different usage in a realistic compressor and are recommended by GE Aviation to study.

2 The NSV Compressor

A GE axial compressor (GE-C1 case) exhibits a NSV at the first stage rotor blades [2]. The first 1-1/2 stage with 56 IGVs, 35 rotor blades and 70 stator blades of the full compressor is used for current simulations. The rotor tip clearance of the compressor rig is 1.1% of tip chord. The measured blade NSV is a phase-locked response and close to 1st torsional blade natural frequency. The strain gage on the blade surface shows a NSV frequency of 2600 Hz at around 12880 rpm and 2661 Hz as the rotor speed slightly decreases to 12700 rpm as shown in Fig. 2. Note that the unsteady pressure measurements either on the blade surface or at the casing are not available.

3 Numerical Methods

The unsteady Reynolds-averaged Navier-Stokes (URANS) equations are solved in a rotating frame [10] with the Spalart-Allmaras (S-A) turbulence model [11]. Shock capturing scheme is necessary to simulate high-speed axial compressors since most rotor blades experience shock/boundary layer interaction. In this study the Low Diffusion E-CUSP (LDE) Scheme [12] as an accurate shock capturing Riemann solver is used with a 3rd order WENO reconstruction for inviscid flux and a 2nd order central differencing for viscous terms [13]. An implicit 2nd order dual time stepping method [14] is solved using an unfactored Gauss-Seidel line iteration to achieve high convergence rate. The high-scalability parallel computing is implemented to save wall clock time [15].

Boundary Conditions

At the IGV inlet, the given radial distributions of total pressure, total temperature, swirl angle and pitch angle are applied and velocity is extrapolated from the computational domain in order to determine the rest of variables. On the blade surface and casing wall a non-slip boundary condition is applied, while on the hub surface the law of the wall is used to avoid an excessive fine mesh in the boundary layer [10]. At the stator outlet, the static pressure is spec-

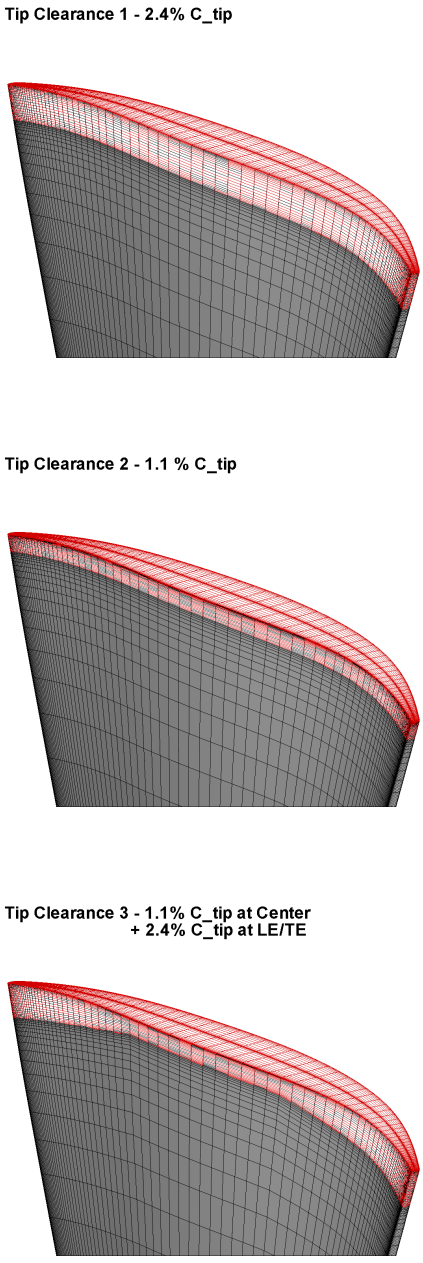

FIGURE 1: Three tip clearances for sensitivity study; plain tip of 2.4% tip chord(top), plain tip of 1.1% tip chord(middle), leading/trailing edge pinched tip of 1.1% tip chord

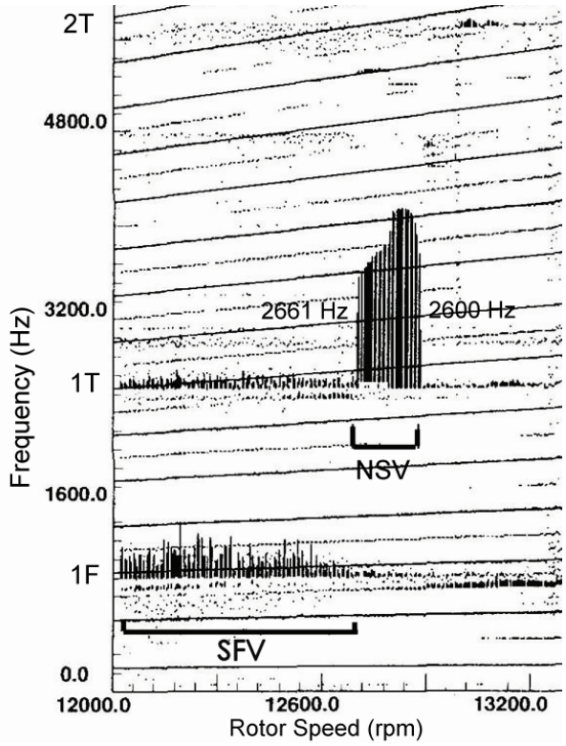

FIGURE 2: Strain gage response of the first-stage rotor blades of the high-speed compressor showing SFV(separated flow vibration) and NSV(non-synchronous vibration)

ified in the spanwise direction. The velocity components are extrapolated from the computational domain and an isentropic relation is used to determine density. If the wall surface is rotating, the wall static pressure for the inviscid momentum equation is determined by solving the radial equilibrium equation. If the wall surface is stationary, the static pressure gradient across the wall boundary is set to zero. In addition, the adiabatic condition is used to impose zero heat flux through the wall. The fully conservative sliding boundary condition (BC) [16] at the blade row interface is used in order to rigorously resolve wake propagation, shocks interaction and rotating instabilities. In addition, an efficient time-shifted phase-lagged BC [17] with nodal diameter of 5 is applied at the lower/upper circumferential periodic boundaries to facilitate 1/7th annulus simulations.

4 Computational Mesh

The 1/7th sector mesh for 1-1/2 stage of the GE-C1 compressor is presented in Fig. 3. The rotor tip clearance is modeled with 21 grid points using an O-mesh block. The mesh of IGV/rotor/stator is partitioned to total 174 blocks for parallel computation. The mesh around blade was constructed by using the O-mesh. For the IGV and stator, 121(around blade)$\times$101(blade-to-blade)$\times$71(blade span) is the mesh size, and for the rotor, 201(around blade)$\times$101(blade-to-blade)$\times$71(blade span). H-mesh layer is used for the matched one-to-one grid point connection at the sliding BC interface of IGV/rotor/stator that enables variable exchange in a fully conservative manner. Each H-mesh layer has a mesh size of 201(tangential)$\times$6(aixal)$\times$71(blade span). The total mesh size for this 1/7 sector of 1-1/2 compressor is 12,127,638. Mesh convergence test was performed using the single passage mixing plane computation and it shows an excellent agreement with GE CFD [16].

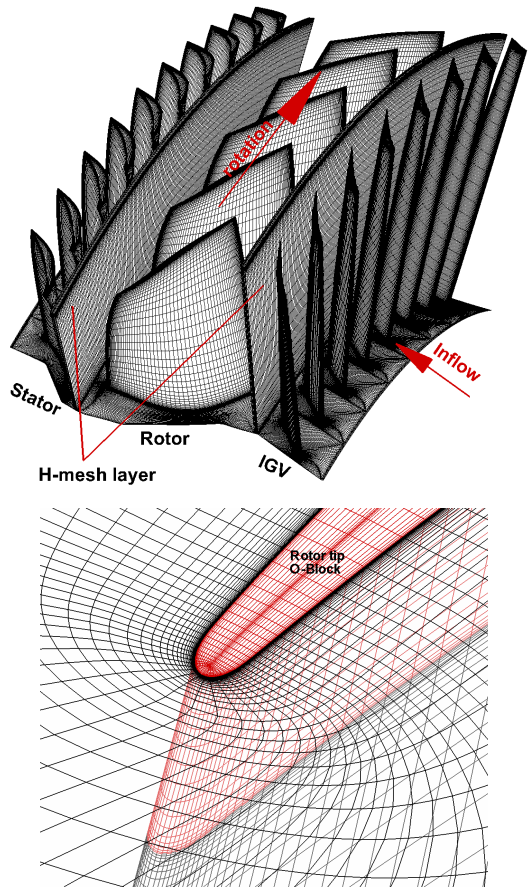

FIGURE 3: 1/7th Annulus mesh for NSV simulation

5 Numerical Probes

The numerical probes to acquire the static pressure responses at the tip clearance are shown in Fig. 4. Total 60 points on a blade surface, 5 points in the middle of tip clearance and 5 points at the casing surface are mounted. The first numeral of the probe number means location around blade surface and the second numeral indicates location of blade span. For example, the probe 64 means the 6th probe from the trailing edge and the 4th probe from the hub, which is on the suction surface of 93% blade span near leading edge.

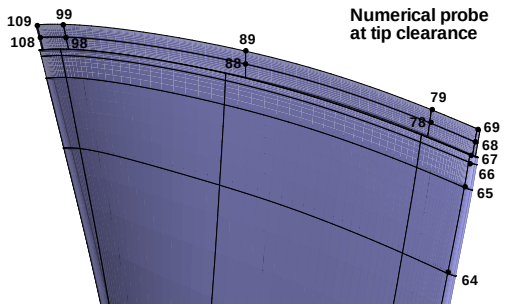

FIGURE 4: Numerical probes of the rotor blade

6 Results and Discussion

The rig testing of the axial compressor with 1.1% tip clearance [2] is shown to have the NSV frequency range of 2600 Hz to 2661 Hz, which is located between 12EOL(engine order line) to 13EOL and is near the 2nd mode blade natural frequency as shown in the Campbell diagram in Fig. 5. The compressor operating point used for the present NSV simulations is 2600 Hz at 12880 rpm. Note that EOL in Campbell diagram is obtained by integer multiples of rotor shaft frequency with respect to rpm. The Campbell diagram can be used to evaluate whether a blade frequency including natural frequency is synchronous or not with engine shaft.

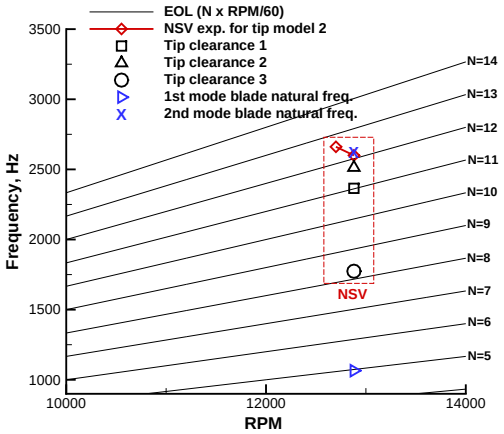

FIGURE 5: Campbell diagram

In this study we conduct the unsteady simulations for the three different tip clearances; 1.1% C_t(tip chord), 2.4% C_t, 1.1% C_t around tip center and 2.4% C_t near LE/TE. The residual is reduced by three orders of magnitude within each physical time step, which is usually achieved within 30 to 40 pseudo time step iterations. A non-dimensional time step of about 0.005 is used.

6.1 The Speedline and NSV Location

Since NSV of axial compressors is typically observed in stable operation [1–4], unsteady flow simulations are first conducted using tip clearance 1 at different back pressure conditions to find NSV dominant region in the speedline. Fig. 6 shows the predicted speedline of the 1-1/2 stage axial compressor. Note that the speedline data in Fig. 6 are obtained by averaging final 2 rotor revolutions. The point A, B, C and D represent rotor-to-IGV total pressure characteristics for tip clearance 1. The back pressure is gradually increased from point S to find the near stall point D. After point D the compressor stalls. The point S is about maximum mass flow condition. No NSV events are found at point S. The mass flow rate obtained at point C is higher by roughly 6% than the near stall point D. GE CFD shows the same frequency for tip clearance 1. The mass flow difference between GE

and the present study is about 2.6%, which may be caused by the fact that GE CFD considers the rotor only without IGV and stator. Note the mass flows predicted by the present CFD and GE CFD are in the close range of the GE-C1 full compressor NSV experiment [2].

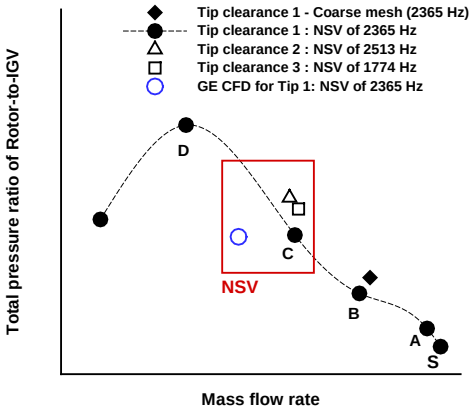

FIGURE 6: Total pressure ratio of IGV-to-Stator versus mass flow rate at the rotor exit

The effect of different tip clearances on the NSV is investigated at point C since the NSV of 2365 Hz with maximum amplitude, which is defined as "peak NSV" in this study, is captured for tip clearance 1. The NSV for tip clearance 2 and tip clearance 3 are obtained by adjusting the back pressure to have about the same mass flow as tip clearance 1. Fig. 7 shows time history of the rotor outlet mass flow rate at point C for tip clearance 1. In this study the unsteady solutions between 1 and 3 rotor revolutions are used for frequency analysis since the predicted mass flows show periodic oscillations roughly after one rotor revolution. The compressor runs stably without flow breakdown during the NSV. However, the flow field at the near stall point D is highly unstable with large mass flow oscillation as shown in Fig .8. In this study the peak NSV frequency of 2365 Hz observed at point C disappears at point D.

6.2 Mesh Refinement Study

The mesh refinement study is conducted at point B using a coarser mesh of 201(around blade)×77(blade-to-blade)×46(blade span) for the IGV, stator and rotor. The total mesh size of the coarse mesh is 6,142,467. As shown in Fig. 6, the total pressure ratio of Rotor-to-IGV and mass flow predicted by the coarser mesh is well converged to the baseline mesh with about 0.5% difference. The IGV passing frequency predicted by the coarser mesh at about 50% span of rotor leading edge shows an excellent agreement with the baseline mesh as presented in Fig. 9.

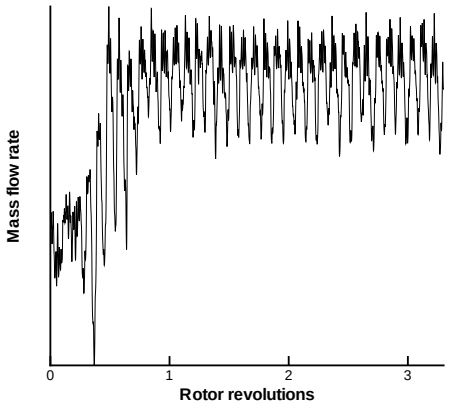

FIGURE 7: History of the rotor outlet mass flow during the NSV for tip clearance 1

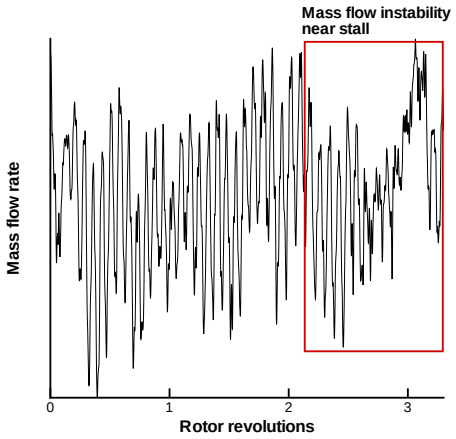

FIGURE 8: History of the rotor outlet mass flow at point D(near stall) for tip clearance 1

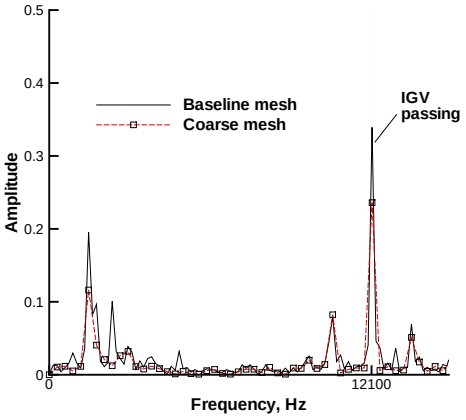

FIGURE 9: Predicted IGV passing frequencies for tip clearance 1 at point B from the mesh refinement test

6.3 NSV for 2.4% Tip Clearance

As aforementioned, for tip clearance 1, a peak NSV frequency of 2365 Hz is observed at point C. All of the static pressure presented and used for frequency analysis in this study are normalized by the IGV inlet dynamic pressure($\rho_\infty U_\infty^2$).

Fig. 10 shows instantaneous fluctuations of the static pressure on the rotor blade 3. Note that the blade is numbered in the opposite direction of the rotor rotation. It is observed in this study that the peak pressure fluctuations occur near rotor leading edge. It is obvious that the largest amplitude of the pressure oscillation is captured at 78% span near the rotor leading edge(probe 63), while the pressure measurements in the tip clearance shows a weak fluctuation. It should be emphasized by the NSV experiment of Baumgartner et al. [1] that the hot-film measurements show the radial dependency of the rotating instability as the main driver of the NSV observed for the 10 stage high pressure axial compressor. The NSV with high blade vibration amplitude is observed between 65% to 91% of the blade span, while the measurements close to the casing wall are very noisy without high fluctuations.

The pressure fluctuations acquired at blade 3 78% span leading edge suction surface at different mass flow is presented in Fig. 11. It is clear that fluctuation level of the pressure is significantly amplified at point C. It is shown by the experiment of Marz et al. [3] that the blade sensor signal under the NSV has a strong periodic content due to the rotating instability. The present numerical simulations also demonstrate a strong periodic signal of the blade surface pressure during the NSV. However, the phase-locked oscillation of the peak NSV pressure signal at point C is changed as a non-cyclic pattern at near stall point D. It is indicated by the NSV experiments [2, 6] that a high speed axial compressor can face the shift of NSV frequencies according to operating conditions.

In Fig. 12, the changes in the NSV frequencies at 78% span at different mass flow conditions are clearly captured with frequency analysis using the pressure signals in Fig. 11. A NSV of 2365 Hz for tip clearance 1 is captured at point C, while at point D a NSV of 2808 Hz, which is between 13EOL and 14EOL, is captured with about 20% lower amplitude than the NSV at point C. At point B, the frequency of 2365 HZ which is the same as point C is obtained with about 50% lower amplitude than the point C. At point D, the NSV frequency of 2365 HZ is ddecaying with its amplitude level about 83% lower than the point C.

Fig. 13 shows the instantaneous pressure signals of 5 rotor blades between 2 and 2.5 Rev acquired at 78% span near leading edge at point C (peak NSV of 2365 Hz with maximum amplitude). The pressure fluctuations of each blade is very similar with about the same frequency, which can indicate a local flow instability. If the instability is propagated to the next blade in a form of traveling wave like a spike stall cell, the phase difference in the acquired blade surface pressure must be in order [18]. However, the phase difference observed in Fig. 13 is disordered between blades. It is shown in the present study that the flow instability as the cause of the NSV is a tip vortex instability that oscillates and interacts with the main flow near the 78% span rotor leading edge.

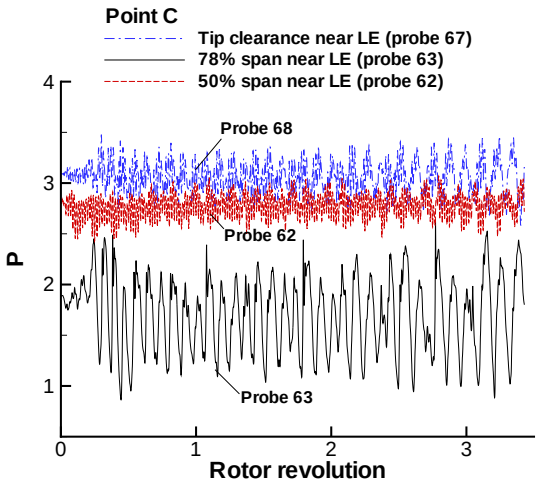

FIGURE 10: Pressure signals acquired at blade 3 leading edge(LE) suction surface for tip clearance 1

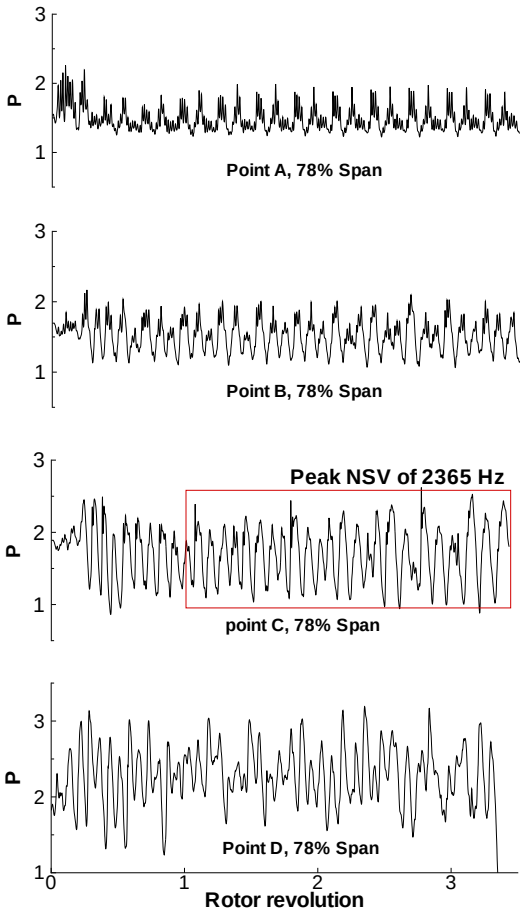

FIGURE 11: Changes in the surface pressures at blade 3 78% span near LE at different mass flows for tip clearance 1

Fig. 14 illustrates the instantaneous tip vortex structure above 78% span of a rotor blade at 3 Rev. A large vortex oscillating with the blade passage is a tornado like vortex with its axis normal to the blade suction surface around the rotor leading edge, which is very different from the common streamwise tip clearance vortex. As illustrated in Fig. 15, the tornado tip vortex exists in each blade passage and results in the same NSV frequency shown in Fig. 16.

Fig. 17 shows the instantaneous entropy contour at near the rotor leading edge axial plane. Entropy is significantly increased around the tornado vortices. Fig. 18 shows the instantaneous axial velocity contour at the rotor tip span. There is a strong interaction between the IGV and rotor due to the tip vortices. Although the flow in the vicinity of the rotor tip is stalled, the high speed compressor runs without the mass flow breakdown during the NSV.

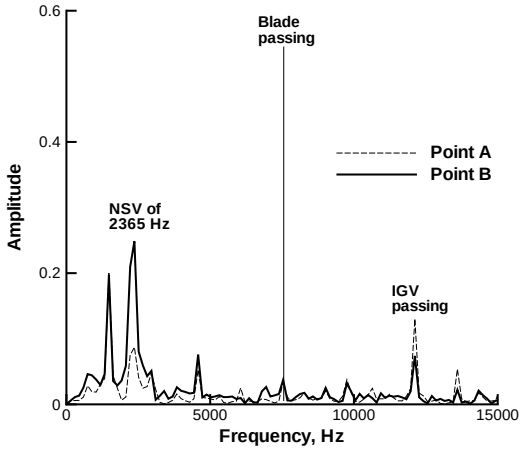

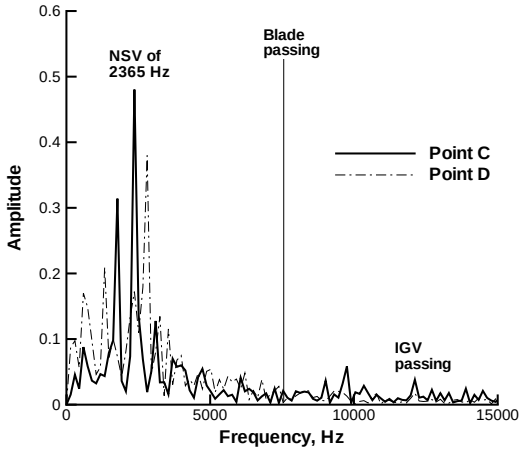

FIGURE 12: Predicted NSV frequencies at blade 3 78% span near LE suction surface for tip clearance 1

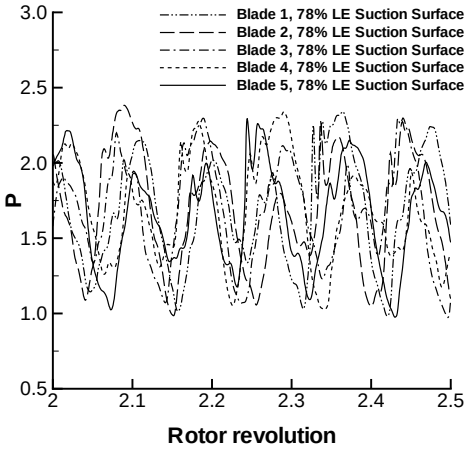

FIGURE 13: Surface blade pressure fluctuations between 2 Rev and 2.5 Rev acquired at 78% span near LE suction surface for tip clearance 1

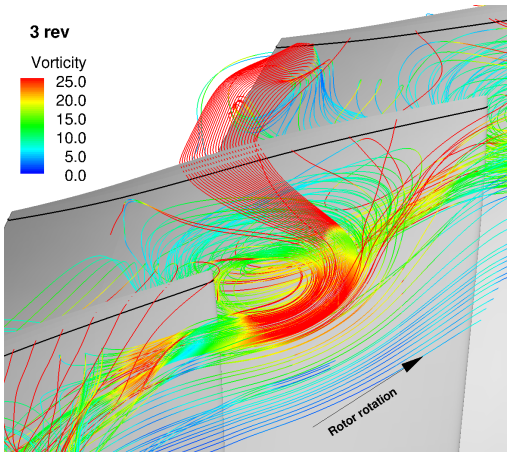

FIGURE 14: Structure of tornado tip vortex at 3 Rev colored with vorticity for tip clearance 1

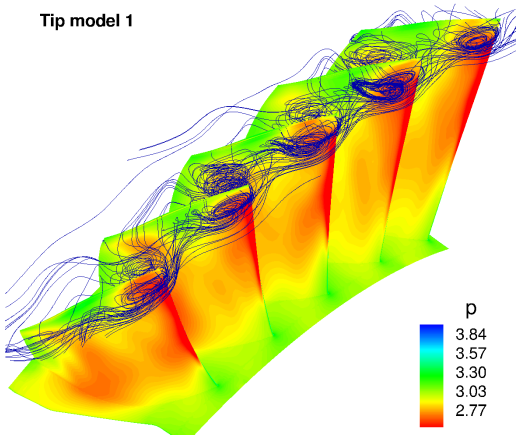

FIGURE 15: Tornado tip vortices in the blade passages during the NSV of 2365 Hz for tip clearance 1

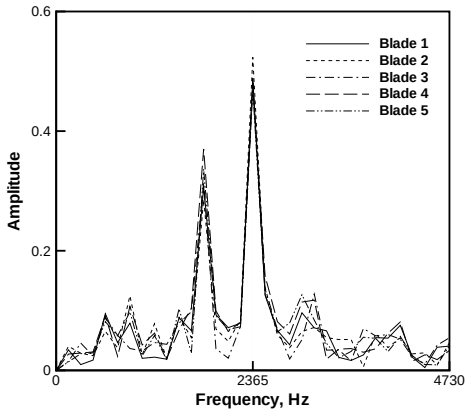

FIGURE 16: Predicted NSV frequencies at 78% span near LE suction surface of tip clearance 1

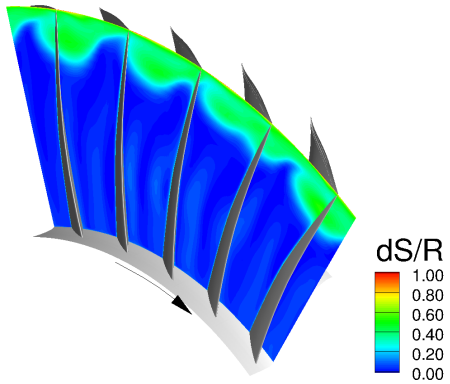

FIGURE 17: Instantaneous entropy contour at near the rotor leading edge axial plane for tip clearance 1

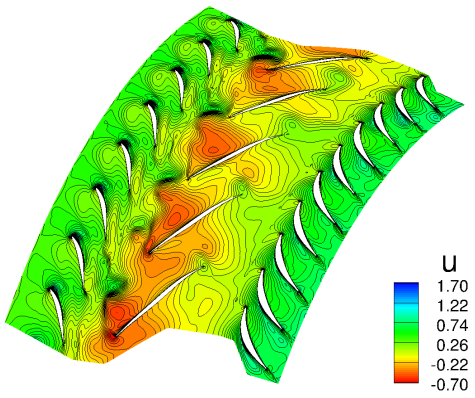

FIGURE 18: Instantaneous axial velocity (U) contour near the rotor tip span for tip clearance 1

6.4 Effect of Rotor Tip Clearance on NSV

To study tip clearance effect on the NSV, tip clearance 2 with 1.1% tip chord(C_t) and tip clearance 3 with 1.1% C_t around tip center and 2.4% C_t near LE/TE as sketched in Fig. 19 are simulated at about the same mass flow where the dominant NSV of 2365 Hz is found for tip clearance 1.

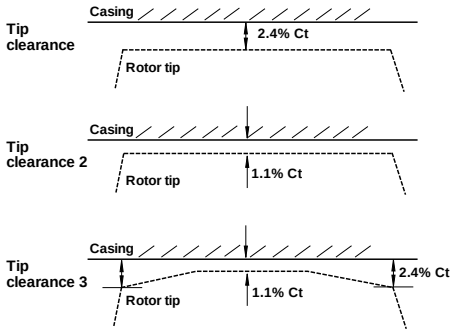

FIGURE 19: Sketch of rotor tip clearance shapes

Instantaneous blade surface pressures at 78% span near LE(probe 63) for tip clearance 1, 2 and 3 are plotted in Fig. 20. Oscillations in the surface pressures are different between tip clearance shapes. The pressure signals for tip clearance 1, 2 and 3 show a periodical and phase-locked pattern but different frequencies.

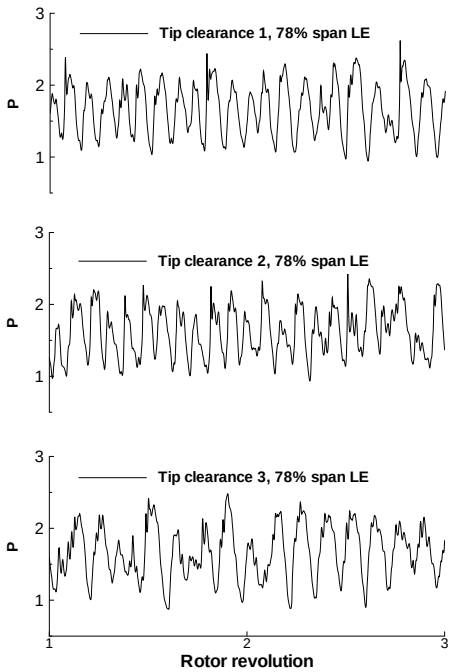

FIGURE 20: Instantaneous surface pressure signals acquired at blade 3 78% span near LE suction surface

Fig. 21 shows the predicted NSV frequencies using the pressure signals in Fig. 20. The dominant frequencies for tip clearance 1, 2 and 3 are 2365 Hz, 2513 Hz and 1774 Hz respectively. Those frequencies are not synchronous to the engine rotor as presented in Fig. 5. The predicted NSV frequency from tip clearance 2 matches the measured value very well, only 3.3% lower. Tip clearance 2 is the one tested in the NSV experiment by GE [2]. Tip clearance 3 shows the peak NSV at 1774 Hz with a significant increase in amplitude by about 42% compared with tip clearance 2. It means that tip clearance 3 generates lower and stronger NSV frequency than tip 1 and 2. It is found that the tip clearance of the compressor rotor changes the NSV frequency and the intensity as well. The straight rotor tip, which are tip clearance 1 and 2, shows smaller amplitude but higher frequency at about the same mass flow condition during the NSV caused by the tornado vortex instability.

The NSV frequencies for tip clearance 1, 2 and 3 at the rotor tip LE are plotted in Fig. 22. The predicted frequencies are the same as those of 78% span near LE suction surface. Except for tip clearance 3, the intensity of the NSV are very weak. It is clear that a convex type of tip clearance 3 amplifies the intensity and reduces the frequency of the NSV.

The distributions of axial velocity(U) at the tip is shown in Fig. 23. The negative axial velocity at X/L of about 0.2(the mid-point of the tip chord) for tip clearance 3 is increased significantly compared with tip clearance 2. Recall that the size of tip clearance 2 and 3 are equal around the mid-chord as sketch in Fig. 19. The pinched tip around leading and trailing edge induces much stronger reversal flow than the straight tip. Hence, the interaction with incoming flow can create a serious flow blockage for tip clearance 3. For the straight tip, the larger clearance of tip 1 shows the larger negative axial velocity than tip 2, which may be a reason why NSV with a straight rotor tip usually becomes dominant with a relatively large tip clearance [3,4].

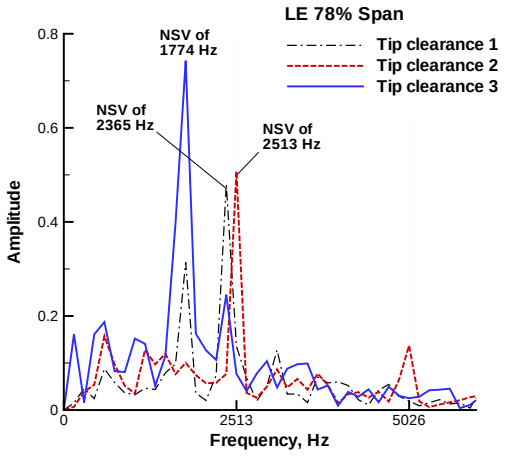

FIGURE 21: Predicted NSV frequencies for tip clearance 1, 2 and 3 at 78% span near LE

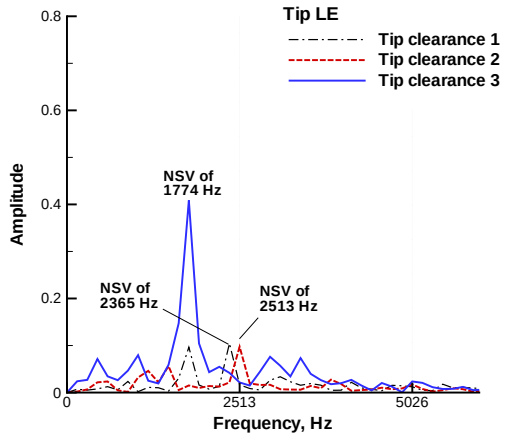

FIGURE 22: Predicted NSV frequencies for tip clearance 1, 2 and 3 at the rotor mid-tip clearance

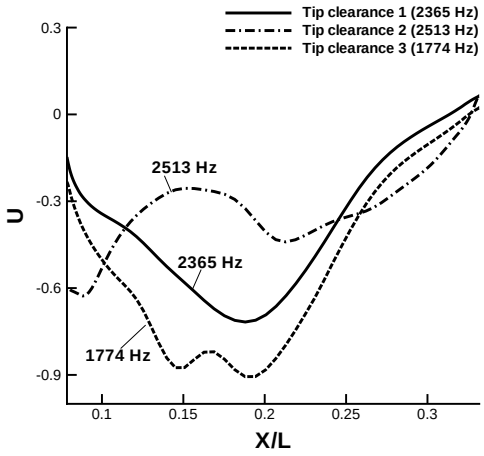

FIGURE 23: Distributions of the tip axial velocity U with respect to the normalized tip axial chord for tip clearance 1, 2 and 3

For tip clearance 2 and 3, the tip tornado vortices similar to tip clearance 1 are also observed during the NSV as shown in Fig. 24. In the region of 78% span, there exists a strong interaction of incoming flow, tip tornado vortices and tip leakage flow, which appears to be the instability causing the NSV. It is shown that the vorticity near 78% span leading edge is the highest. Fig. 24 also indicates that the tip tornado vortex of a blade is not formed primarily by its own tip leakage jet, but by the tip leakage jet from the adjacent upstream blade and the jet interaction with the incoming flow. Tip clearance 3 that is more open at LE and narrow at mid-chord appears enhancing the tip leakage jet and blockage, which increases the intensity of the tornado vortices and decreases the NSV frequency.

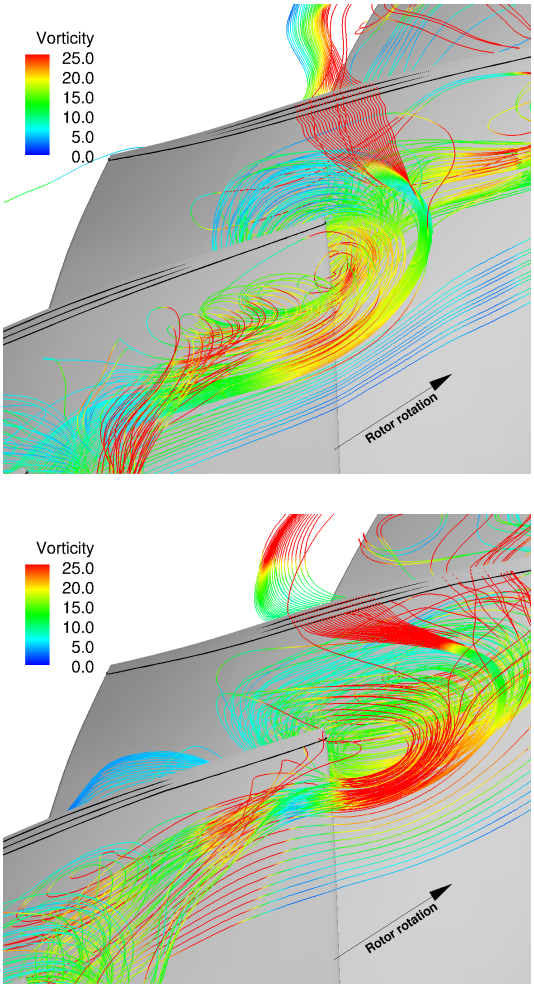

FIGURE 24: Tornado like tip vortex colored with vorticity ar 3 Rev; tip clearance 2(top), tip clearance 3(bottom)

To investigate the effect of tip leakage impinging jet acoustic resonance on the NSV, the NSV critical tip velocity (Eq. 1) based on their impinging jet experiment suggested by Thomassin et al. [5,6] is calculated.

$$U_{tipc} = 2(c - 2sf_b/n) \tag{1}$$

In the above equation, c is speed of sound at tip clearance, s the blade pitch, f_b the blade natural frequency and n the integer of harmonics for the acoustic feedback wave. The critical velocity(U_{tipc}) is estimated at tip clearance center(the probe 87).

For tip clearance 1, the blade natural frequency(f_b) near the NSV is about 2620 Hz, the local speed sound is about 349.5 m/s. The calculated U_{tipc} with $n = 1$ is 227.2 and with $n = 2$ is 463.1, while the blade tip velocity(U_{tip}) measured is about 340.5 m/s. The calculated NSV critical velocity(U_{tipc}) based on Eq.1 is about 33% lower than U_{tip}. For tip clearance 2, the local speed sound is about 355.3 m/s. U_{tipc} of 236.7 with $n = 1$ and of 473.7 with $n = 2$ are obtained, while U_{tip} is 341.4 m/s. The calculated value of U_{tipc} with $n = 1$ is roughly 30% lower than U_{tip}. Similar results are also obtained for tip clearance 3. Since the condition of the NSV driven by tip leakage acoustic resonance is $U_{tipc}/U_{tip} \approx 1$, it appears that the acoustic wave of tip leakage jet is not responsible for the NSV observed in this study.

6.5 Estimation of Tip Vortex Passing Frequency

It is found that the the tornado tip vortex instability near the rotor tip plays a dominant role in the NSV event observed in this study. To investigate the mechanism behind the NSV, the tornado vortex structure of tip clearance 2, which is the experimental model with the NSV at 2600 Hz, is inspected at eight time instants from 2 Rev to$2 + \frac{7}{70}$ Rev as illustrated in Fig. 25 and Fig. 26. Note all figures are rotated in the opposite direction of rotor rotation for comparison at the same location.

It is clear that the tornado vortex structure originated from the rotor leading edge suction surface travels in the streamwise direction. The tornado vortex at 2 Rev is replaced with another identical one after roughly $\frac{6}{70}$ Rev, which indicates the period of the traveling tornado vortex is about 11.7 times shorter than the rotor revolution. Therefore, the passing frequency of the tornado vortex roughly matches the NSV of 2513 Hz acquired at the rotor leading at 78% span.

7 Conclusions

Numerical simulation is conducted to investigate the NSV mechanism for a GE axial compressor. A 1/7th annulus of a 1-1/2 stage is used with a fully conservative sliding BC at blade row interfaces and a time shift boundary condition at the lower/upper circumferential periodic boundaries. A 3D URANS solver with a low diffusion Riemann solver, 3rd Order WENO scheme, S-A turbulence model is used.

A tornado like tip vortex structure moving in the streamwise direction with vortex axis normal to the blade suction surface is observed during the NSV near the rotor tip region for all tip clearances studied. The passing frequency of the tip vortex roughly matches the NSV frequency. The streamwise oscillation of these tornado vortices due to the strong interaction with incoming flow, tip vortex and tip leakage flow appears to be the main cause of the NSV observed in this study.

Three different tip clearances are studied. Tip clearance 1 and 2 are designed to have a straight tip clearance with the clearance size of 1.1% and 2.4% tip chord respectively, while tip clearance 3 has a convex type tip with clearance of 1.1% tip chord around tip center and 2.4% tip chord near LE/TE.

The present study accurately predicts the peak NSV of 2513 Hz for a straight tip of 1.1% tip clearance, which is about 3.3% lower than the experiment. As the rotor tip clearance is increased to 2.4% without shape change, the dominant NSV frequency is reduced by about 6% with the pressure oscillation amplitude slightly reduced. However, when the tip shape is changed to tip clearance 3, the peak NSV frequency is reduced by about 29% with a significant increase in pressure oscillation amplitude by about 42%.

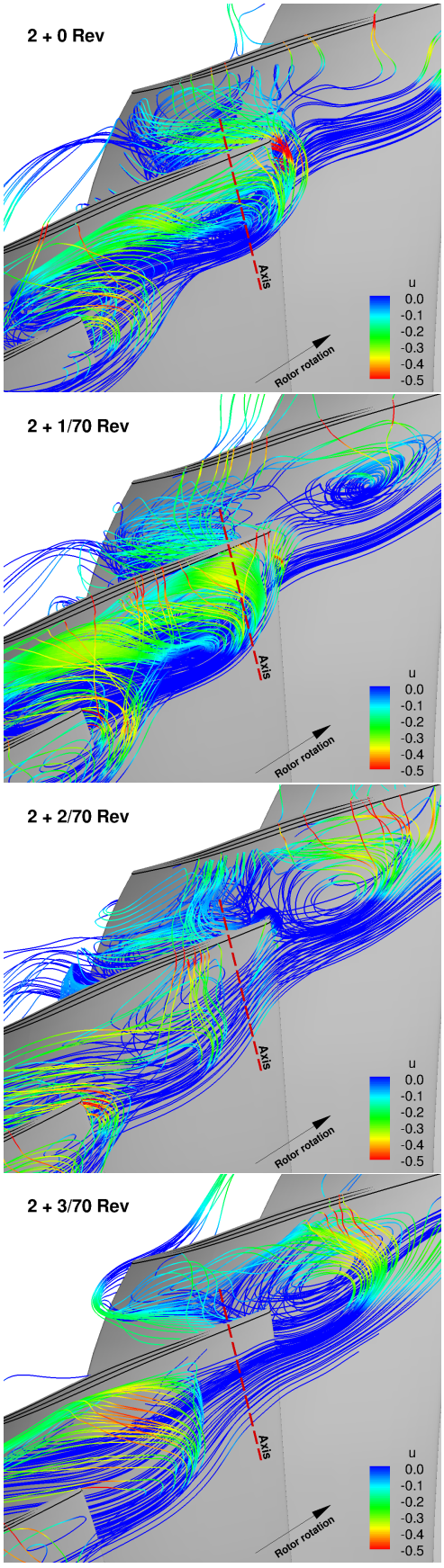

FIGURE 25: Instantaneous tip vortex trajectories for tip clearance 2 at 2, 2+1/70, 2+2/70, 2+3/70 Rev colored by the negative axial velocity.

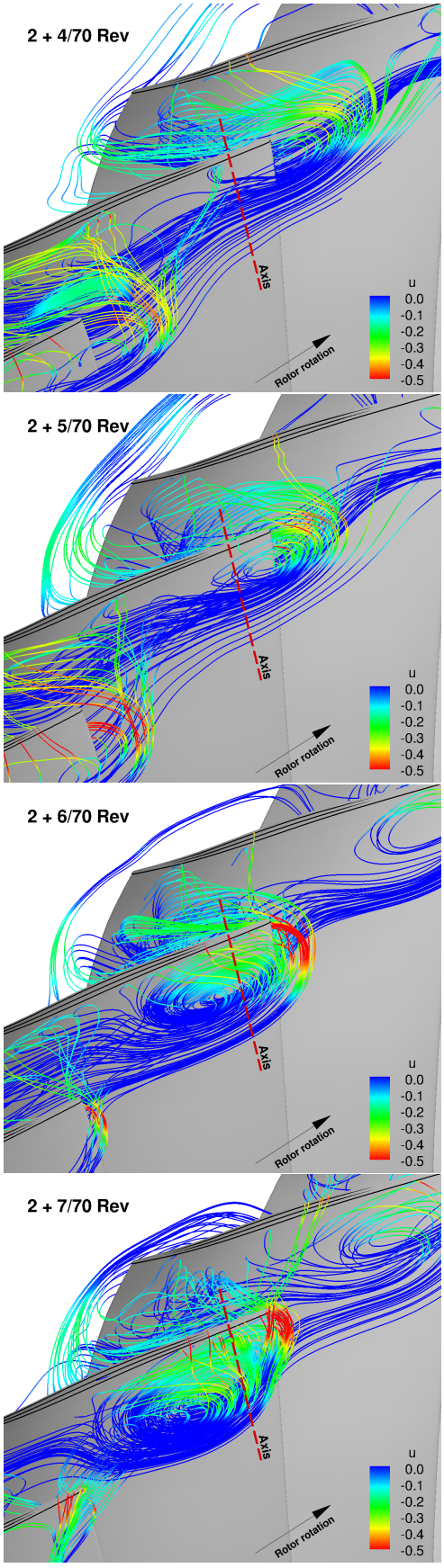

FIGURE 26: Instantaneous tip tornado vortex trajectories for tip clearance 2 at 2+4/70, 2+5/70, 2+6/70, 2+7/70 Rev colored by the negative axial velocity.

Nomenclature

C_t	blade tip chord
L	reference length used for normalization
P	normalized static pressure by inlet dynamic pressure, $\rho_\infty U_\infty^2$
$\frac{\Delta S}{R}$	change of entropy, $\frac{\gamma}{\gamma-1} ln \frac{To}{To_\infty} - ln \frac{Po}{Po_\infty}$
T	normalized static temperature
U	normalized axial velocity
$WENO$	Weighted Essentially Non-oscillatory

- Subscripts -

$_o$	stagnation property
$_\infty$	reference point

Acknowledgement

We thank GE for approving publishing the results. We greatly appreciate the help of Gerardo "LC" Colmenero and Steve Manwaring at GE Aviation for providing the compressor geometry and testing data. The grants support from AFRL and the industrial partners of GUIde Consortium, 10-AFRL-1024 and 09-GUIDE-1010, are acknowledged. The numerical simulations are conducted at the Center for Computational Sciences at the University of Miami and Air Force Research Lab DoD High Performance Computing Centers.

REFERENCES

[1] M. Baumgartner, F. Kameier, and J. Hourmouziadis, "Non-Engine Order Blade Vibration in a High Pressure Compressor." ISABE, Twelfth International Symposium on Airbreathing Engines, Melbourne, Austrlia, 10-15, 1995.

[2] R. Kielb, J. Thomas, P. barter, and K. Hall, "Blade Excitation by Aerodynamic Instabilites - A Compressor Blade Study." ASME Paper No. GT-2003-38634, 2003.

[3] J. Marz, C. Hah, and W. Neise, "An Experimental and Numerical investigation Into the Mechanisms of Rotating instability," *Journal of Turbomachinery*, vol. 124, pp. 367–375, 2002.

[4] R. Mailach, I. Lehmann, and K. Vogeler, "Rotating Instabilites in an Axial Compressor Originating From the Fluctuating Blade Tip Vortex." ASME Paper No. GT-2003-38634, 2003.

[5] J. Thomassin, H. Vo, and N. Mureithi, "Blade Tip Clearance Flow and Compressor Nonsynchronous Vibrations: The Jet Core Feedback Theory as the Coupling Mechanism," *Journal of Turbomachinery*, vol. 131, pp. 11013–1–11013–9, 2009.

[6] J. Thomassin, H. Vo, and N. Mureithi, "The Tip Clearance Flow Resonance Behind Axial Compressor Nonsynchronous Vibration," *Journal of Turbomachinery*, vol. 133, pp. 041030–1–041030–10, 2011, doi:10.1115/1.4001368.

[7] A. Sanders, "Nonsynchronous Vibration(NSV) due to a Flow-Induced Aerodynamic Instability in a Composite Fan Stator," *Journal of Turbomachinery*, vol. 127, pp. 412–421, 2005.

[8] Vo, H.D., "Role of Tip Clearance Flow in Rotating Instabilities and Nonsynchronous Vibrations," *Journal of Propulsion and Power*, vol. 26, pp. 556–561, doi: 10.2514/1.26709, 2010.

[9] A. Carter, and D. Kilpatrick, "Self-excited vibration of axial-flow compressor blades," *Proceedings of the Institution of Mechanical Engineers 1847-1996*, vol. 171, pp. 245–281, 1957, DOI:10.1243/PIME_PROC_1957_171_030_02.

[10] H.S. Im, X.Y. Chen, and G.C. Zha, "Detached Eddy Simulation of Rotating Stall for a Full Annulus Transonic Rotor," *submitted to Journal of Propulsion and Power, 2011-07-B34395*, 2011.

[11] P.R. Spalart, W.H. Jou, M. Strelets, and S.R. Allmaras, "Comments on the Feasibility of LES for Wings, and on a Hybrid RANS/LES Approach." Advances in DNS/LES, 1st AFOSR Int. Conf. on DNS/LES, Greyden Press, Columbus, H., Aug. 4-8, 1997.

[12] G.C. Zha, Y.Q. Shen, and B.Y. Wang, "An improved low diffusion E-CUSP upwind scheme ," *Journal of Computer and Fluids*, vol. 48, pp. 214–220, 2011, doi:10.1016/j.compfluid.2011.03.012.

[13] Y.Q. Shen, G.C. Zha, and B.Y. Wang, "Improvement of Stability and Accuracy of Implicit WENO Scheme," *AIAA Journal*, vol. 47, pp. 331–334, DOI:10.2514/1.37697, 2009.

[14] Y.Q. Shen, B.Y. Wang, and G.C. Zha, "Implicit WENO Scheme and High Order Viscous Formulas for Compressible Flows ." AIAA Paper 2007-4431, 2007.

[15] B. Wang, Z. Hu, and G. Zha, "A General Sub-Domain Boundary Mapping Procedure For Structured Grid CFD Parallel Computation," *AIAA Journal of Aerospace Computing, Information, and Communication*, vol. 5, pp. 425–447, 2008.

[16] H.S. Im, X.Y. Chen, and G.C. Zha, "Simulation of 3D Multistage Axial Compressor Using a Fully Conservative Sliding Boundary Condition." ASME IMECE2011-62049, International Mechanical Engineering Congress & Exposition, Denver, November 2011, 2011.

[17] H.S. Im, and G.C. Zha, "Simulation of Nonsynchronous Blade Vibration of an Axial Compressor Using a Fully Coupled Fluid/ Structure Interaction." ASME GT2012-68150, 2012.

[18] H. Im, X. Chen, and G. Zha, "Detached Eddy Simulation of Unsteady Stall Flows of a Full Annulus Transonic Rotor." AIAA Journal of Propulsion & Power, to appear.